Original Article

JSA

J Strain Analysis
1–12

DOI: 10.1177/0309324714525146
sdj.sagepub.com
SAGE

A two-parameter approach to assess effects of constraint in cracks located at geometrical discontinuities

Guilherme Victor P Donato[1], João Marcos A Rebello[2] and Cláudio Ruggieri[3]

Abstract

This work provides an exploratory investigation into the applicability of a two-parameter fracture mechanics approach based on the *J-Q* methodology to characterize fracture behavior in cracks located at geometrical discontinuities of pressure vessels submitted to pressurization and depressurization cycles. Numerical models in plane-strain condition were employed to characterize crack driving forces and constraint changes in a flawed structure subjected to shakedown. The material exhibits elastic–plastic behavior and nonlinear kinematic hardening following the Chaboche model. The results indicate that the application of cycles of loading exceeding elastic limits, but still below the allowable stress for design of pressure vessels, increases the crack driving force and decreases the constraint level. It is possible to conclude that the methodology based on *J-Q* is highly effective to characterize the fracture conditions in geometrical discontinuities of pressure vessels. A lower probability of unstable fracture may be assumed for ductile and high-toughness materials after few cycles of pressurization and depressurization are applied. However, due to the increase in the driving force, the crack may be more susceptible to a subcritical tearing. Assuming that the material toughness is high enough to avoid any ductile tearing during pressurization and depressurization cycles, the observed phenomena close to the crack tip may be compared to instability of strains when shakedown is not guaranteed.

Keywords

Constraint, *J-Q* methodology, shakedown, pressure vessels, pressure test, geometrical discontinuities

Date received: 28 July 2013; accepted: 21 January 2014

Introduction

Refineries and chemical processing plants consist essentially of pressurized equipment, such as pressure vessels and piping, which require high reliability in their design and fabrication. Fail-safe operation of these plants relies directly on the application of structural integrity assessment procedures and correct predictions of failure conditions for in-service cracked structures. The specification of critical flaw dimensions and the allowable limits of the various types of damages is fundamental for repair decisions and life extension of these facilities. Conventional fracture mechanics approaches to assess the significance of crack-like defects in pressurized equipment, including high pressure vessels, build upon a fundamental concept in which a single parameter defining the crack driving force is used. The *Mode I* elastic stress intensity factor K_I[1,2] or the elastic–plastic *J*-integral[3] and the crack-tip opening displacement (CTOD)[4] describe the (local) conditions for the material's failure. Given the condition that such one-parameter methodology describes the near-tip stress and strain fields ahead of the crack, the approach yields a very effective defect acceptance procedure for mechanical and structural components, which can then be used to establish operating conditions in terms of admissible applied loads or crack sizes.

[1]Materials, Corrosion and Equipment Group, Research and Development Center (CENPES), PETROBRAS (Brazilian Oil Company), Rio de Janeiro, Brazil
[2]Department of Metallurgy and Materials Engineering, Federal University of Rio de Janeiro, Rio de Janeiro, Brazil
[3]Department of Naval Architecture and Ocean Engineering, University of São Paulo, São Paulo, Brazil

Corresponding author:
Guilherme Victor P Donato, Materials, Corrosion and Equipment Group, Research and Development Center (CENPES), PETROBRAS (Brazilian Oil Company), Horacio de Macedo Avenue, 950, Ilha do Fundão, Rio de Janeiro 21941-915, Brazil.
Email: donato@petrobras.com.br

However, crack-like flaws often occur at geometrical discontinuities and stress concentration regions such as nozzle connections, openings and head shell junctures in pressure vessels. With increased loading, these regions undergo severe plastic deformation well beyond the elastic limits of the material with strong impact on damage accumulation in the neighborhood of a crack-tip flaw. A case of interest related to the occurrence of plastic strains at geometrical discontinuity regions is the shakedown phenomenon in elastic plastic structures.[5–10] During service and after an initial short-term transient response, pressurization cycles subject the pressure vessel to repetitive loading, which causes reverse plasticity and plastic accommodation of material leading the structure to elastic behavior in subsequent operations. The changes in the local stress and strain fields due to plastic shakedown affect the coupling relationship between macroscopic loading and the crack-tip driving force as characterized by the J-integral, thereby compromising accurate defect assessments based upon a single-parameter fracture mechanics approach.

The history of construction of welded pressure vessels has been of continuous developments in design, fabrication techniques and new materials. Earlier pressurized equipments were made of low toughness and low ductility materials with relatively reduced structural capacity with increased applied pressure arising from the development of high levels of plastic strain in high-stress concentration regions or ahead of crack-like defects. When subjected to a hydrostatic pressure testing to guarantee safety and fabrication standards, a pressure vessel containing a sharp crack-like flaw would not withstand the applied load and would fail at a relatively low pressure, thereby preventing a flawed structural component from going into service. However, it is changing gradually over recent years. Nowadays, the hydrostatic pressure test may be considered as limited for evaluating the importance of cracks or flaws. Structural steels currently used for the fabrication of pressure vessels have much higher strain capacity and fracture resistance. As a consequence of this improvement of properties, a sharp crack that might occur in the structure could undergo large applied loads without failure. Consequently, the pressure test may prove inadequate for accurately evaluating structural integrity when assessing gross manufacturing errors and, perhaps even more important, the mechanical integrity of old or even new pressure vessels.

The potentially reduced effectiveness of hydrostatic pressure testing within the scenario previously described increases the probability of failure and the consequences of undetected defects, especially critical crack-like flaws located at a geometric discontinuity of a pressure vessel submitted to a few pressurization cycles. Furthermore, a more critical condition may occur in which a crack may grow stably without failure during cycles of pressurization and depressurization. Such condition is likely to represent a potential problem for the useful lifetime of the pressure vessel and a high operational risk. Moreover, the material ahead of these cracks undergoes stress and strain changes during shakedown of the structure and a strong constraint loss associated with plastic process at the crack tip, which may prevent an unstable material failure. Clearly, the history effects of deformation associated with the shakedown process of the structure which thereby influences the near-tip stress and strain fields should be considered when developing more accurate fracture mechanics methodologies applicable to defect assessments of pressure vessels subjected to repeated loading.

This work explores further extensions of concepts of a bi-parametric fracture mechanics approach based on the J-Q methodology to assess effects of pressure cycles and shakedown process on the alterations of crack-tip constraint in crack-like flaws located in geometrical discontinuities. A central objective is to evaluate the fracture behavior of cracks located in geometrical discontinuities of pressure vessels submitted to alternating membrane and bending stresses. Plane-strain finite element analyses were performed on a cracked beam model representing low- and high-constraint conditions to simulate pressurized components with varying levels of stiffness. The results indicate that the crack driving force increases and constraint level decreases when cycles of loading exceeding elastic limits but still below the allowable stress for design of pressure vessels are applied. A lower probability of unstable fracture may be assumed for ductile and high-toughness materials after few cycles of pressurization and depressurization are applied; however, the crack may be more susceptible to a subcritical tearing due to increased crack driving force. Assuming that the material toughness is high enough to avoid any ductile crack tearing during pressurization and depressurization cycles, the intense elastic plastic process close to the crack tip may be associated with strain instability when shakedown is not guaranteed. This condition may occur even if strain stabilization (shakedown) takes place in the structure (which behaves in an elastic manner after applying few cycles of loading).

Shakedown in geometrical discontinuities

High levels of stress and strain may occur in regions of geometric discontinuities of pressure vessels when submitted to internal pressure. The reason for this is related to differences in stiffness between welded components of different geometries and the resulting incompatibility of displacements and rotations at boundary limits in these components.

Compatibility of displacements and rotations arises from the membrane and bending stresses developed during application of internal pressure followed by material accommodation. According to the *ASME Boiler and Pressure Vessel Code*,[11] membrane stresses at

geometric discontinuities are usually classified as localized primary stress (named P_L). The allowable limit of P_L is the material's yield strength in order to avoid plastic collapse of the section. Bending stresses are classified as a secondary quantity self-limited by plastic deformation (named Q). Considering a conventional elastic stress analysis, the limit of primary stress added to the secondary stress corresponds to twice the yield strength, which represents the theoretical limit for shakedown of elastic perfectly plastic materials. As the consequence of such limits, the pseudo-elastic stress along the section of the structure varies from twice of the yield strength to zero. However, due to the elastic plastic behavior and by virtue of the material's constitutive formulation, the character of the actual stress distribution is different than the corresponding (assumed) character of pseudo-elastic stresses which in turn causes the development of larger plastic strains associated with higher levels of stresses.

It is important to observe that the character of near-tip stress and strain fields is different than the corresponding character of the global (macroscopic) stresses. While global stabilization of stress and strains is likely to occur when the structure behaves in an elastic manner after a few cycles of loading, the shakedown in cracked or flawed structural discontinuities is not guaranteed due to a more intense and severe plastic phenomenon at the crack-tip region.

A number of previous works provide some support to such arguments. Stein et al.[12] proposed equation (1) for the stress intensity factor, which may be considered as a threshold value. Therefore, for cyclically applied stress intensity factors greater than the threshold, strain stabilization at or close to the crack tip is not warranted, even if global shakedown occurs. Stein et al.[12] compare such behavior to a fatigue crack growth phenomenon in which the structure remains (globally) elastic but the crack tip "senses" the evolving stress and strain fields under elastic plastic conditions, albeit with limited plasticity

$$K_{sh} = \frac{\sigma_o \sqrt{\pi \rho_{eff}}}{\sqrt{1 - \nu - \nu^2}} \quad (1)$$

where ρ_{eff} represents an effective radius at the crack tip, ν is Poisson's ratio and σ_o is the reference yield strength.

Feng and Gross[13] discussed different possibilities when making comparisons between global (structure) and local (near-tip) shakedown behavior of cracked structures. In agreement with the results presented later in this article, Feng and Gross[13] concluded that the evolving stress and strain fields near the crack tip display an elastic plastic character after some cycles of loading even though the structure remains elastic.

Overview of constraint description based on the J-Q approach

High-constraint reference field based on the modified boundary layer model

The modified boundary layer (MBL) model illustrated in Figure 1 is often used as an alternative convenient approach to represent the theoretical solution of the stress field ahead of a stationary crack in elastic plastic materials under small-scale yielding (SSY). This theoretical solution was initially formulated by Hutchinson,[14,15] Rice and Rosengren[16] and Rice,[17] which is widely known as the HRR solution.[18] The MBL model was originally proposed by Rice[19] and consists of a (very large) circular region containing an edge crack to provide a convenient reference solution for an infinite body. It is used to quantify the effects of finite size on the crack-tip stress fields while simplifying the generation of numerical solutions for stationary cracks under *Mode I* loading. Assuming that the dimensions of the plastic zone close to the crack tip are limited to a small fraction of the model, $R_p \ll R/20$, where R_p is the radius (size) of the crack-tip plastic zone, the stress field beyond the limits of the plastic

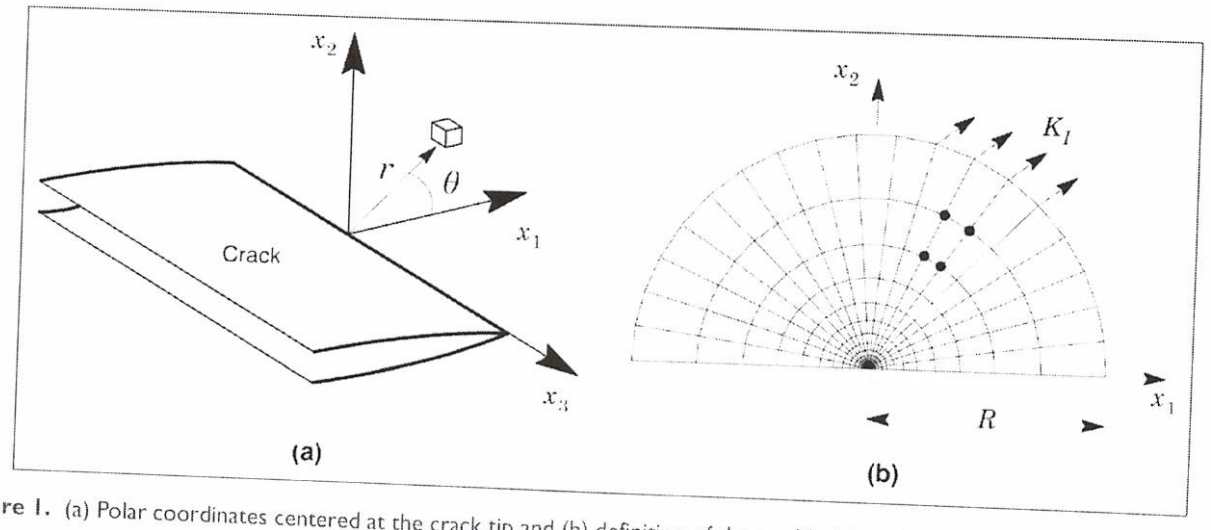

Figure 1. (a) Polar coordinates centered at the crack tip and (b) definition of the modified boundary layer (MBL) problem.

strains region may be represented by an asymptotic equation given by

$$\sigma_{ij} = \frac{K_I}{\sqrt{2\pi r}} f_{ij}(\theta) \tag{2}$$

where K_I is the elastic stress intensity factor, f_{ij} defines the angular variations of in-plane stress components and (r, θ) are polar coordinates centered at the crack tip (see Figure 1).

Numerical analyses for different levels of loading are performed by imposing elastic, *Mode I* displacements on the extremities of the model. These boundary conditions create an elastic stress field (*Mode I*) on the outer circular boundary ($r = R$), which involves the crack in the form

$$u(R,\theta) = \frac{K_I(1-\nu)}{E}\sqrt{\frac{R}{2\pi}}\cos\left(\frac{\theta}{2}\right)(3-4\nu-\cos\theta) \tag{3}$$

$$v(R,\theta) = \frac{K_I(1-\nu)}{E}\sqrt{\frac{R}{2\pi}}\sin\left(\frac{\theta}{2}\right)(3-4\nu-\cos\theta) \tag{4}$$

where E is the material elasticity modulus and ν is Poisson's ratio.

The Q parameter

Much research and previous experimental studies have shown significant increase in the elastic plastic fracture toughness (as characterized by J_c or CTOD) for shallow crack configurations and tension loaded geometries of common structural steels in the ductile-to-brittle transition (DBT) region. This apparent increase in experimentally measured fracture toughness observed in the DBT region is often associated with the phenomenon of constraint loss. Under such conditions, larger crack driving forces, as characterized by J, are required to propagate unstably a cleavage micro-crack in the highly stressed region ahead of crack tip.

In analyzing the phenomenon of constraint loss in common fracture specimens, O'Dowd and Shih (OS)[20,21] adopted an approximate solution to describe the elastic plastic crack-tip fields in large-scale yielding (LSY) conditions. This solution is based on two-parameter approach in order to represent low-constraint crack configurations. For materials with elastic plastic response described by a power hardening law given by equation (5) and utilizing a MBL model,[22,23] OS defined the structure of the crack-tip stress fields by equation (6)

$$\varepsilon_p \propto \left(\frac{\sigma}{\sigma_0}\right)^n \tag{5}$$

where ε_p is the plastic strain, n denotes the strain hardening exponent and σ_o is the reference (yield) stress

$$\sigma_{ij} = \sigma_o \bar{f}_{ij}\left(\frac{r}{J/\sigma_o}, \theta, Q\right) \tag{6}$$

where the deviation of the stress field σ_{ij} from a reference SSY solution for fracture test specimens or actual structures is represented by the parameter Q. In equation (6), r and θ are polar coordinates centered at the crack tip with $\theta = 0$ corresponding to the crack plane and with direction to ahead of crack tip.

OS showed that the difference of the stress field for a reference solution may be calculated by $Q\sigma_o$, which corresponds to a uniform hydrostatic stress for a limited range of distance from the crack tip

$$\sigma_{ij} = \sigma_{ij}^{SSY} + Q\sigma_o\delta_{ij}; |\theta| < \frac{\pi}{2}; \frac{J}{\sigma_o} \leqslant r \leqslant \frac{5J}{\sigma_o} \tag{7}$$

Operationally, OS defined Q as

$$Q \equiv \frac{\sigma_{\theta\theta}^{FB} - \sigma_{\theta\theta}^{SSY}}{\sigma_o}; \theta = 0; r = \frac{2J}{\sigma_o} \tag{8}$$

where $\sigma_{\theta\theta}$ is the crack opening stress and $r = 2J/\sigma_o$ is assumed as the critical location for cleavage mechanism ahead of crack tip, and it is usually the distance chosen for the parameter Q definition. Equation (8) is used to generate J-Q trajectories, which follow the changes of load levels applied on the finite body (FB).[24]

Extension of the J-Q approach to include load history effects

An alternative definition for parameter Q is introduced here for the fracture assessments of cracked structural components under variable elastic plastic loading by means of the J-Q methodology, including plastic shakedown. Since the difference of field associated with a high-triaxiality reference stress state characterizes the degree of crack-tip constraint, a more convenient and yet effective measure of Q including load history effects is given by

$$Q \equiv \frac{\sigma_{\theta\theta}^{FB,t=t_k} - \sigma_{\theta\theta}^{SSY,t=0}}{\sigma_o}; \theta = 0; r = \frac{2J}{\sigma_o} \tag{9}$$

where it is understood that the reference stress state derived from the MBL model is evaluated at time $t = 0$ and the finite body stresses are evaluated at time $t = t_k$, thereby reflecting the loading unloading sequences and associated reverse plasticity effects.

The effects of secondary stresses on the crack driving force are recognized by general procedures based on conventional fracture mechanics;[25,26] however, only primary stresses are usually associated with the level of constraint. Since the stress fields for the finite body may incorporate the effects of both primary and secondary stresses, the parameter Q also reflects the difference of the field derived from both the primary and secondary stresses. Hence, within the present methodology, the change in the finite body stress fields can arise from variations in either the primary or secondary stress, or both the stress quantities. Consequently, parameter Q enables assessing the potentially strong

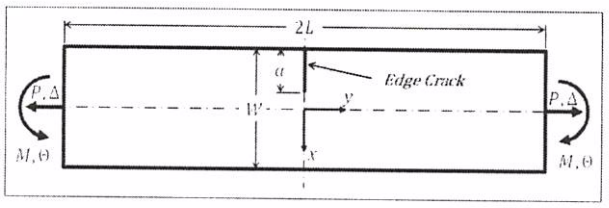

Figure 2. Beam with a single edge crack.

changes in crack-tip constraint associated with the coupled effect of primary and secondary stresses on the problem addressed in this work. In addition, both primary and secondary stresses behave elastically after shakedown in geometric discontinuities of pressure vessels. The secondary stress will be limited by plastic deformation, and it will incorporate characteristics of primary stress with its magnitude proportional to the loading (internal pressure for a pressure vessel).

Computational procedures

Finite element models

A high-constraint reference solution, which represents a SSY condition, was defined by the MBL model displayed previously in Figure 1. The displacements calculated by equations (3) and (4) were applied incrementally in 20 load steps until a maximum stress intensity value of $K_I = 300$ MPa $m^{1/2}$ was attained.

Figure 2 displays a simplified model of a beam subjected to axial and bending loading. This model was used to assess different levels of stress conditions, which typify geometric discontinuities in pressure vessels. This configuration was chosen to simulate actual structures by considering the similarities between the stress fields for the adopted beam model and the allowable stress conditions given by the *ASME Boiler and Pressure Vessel Code*.[11] The beam geometry represents conditions of low and high levels of constraint using two different crack size (a) over beam width (W) ratios of $a/W = 0.20$ (Model 1) and $a/W = 0.50$ (Model 2). The overall dimensions of the model are $W = 50$ mm, $L = 100$ mm and $a = 10$ or 25 mm. By changing the magnitude of the imposed displacement and angular rotation, it is possible to simulate pressurized components with varying levels of stiffness. The results showed in this work represent the maximum stress condition in which the pseudo-elastic stress distribution varies from $2\sigma_o$ to 0 through the beam section.

The displacements and rotations applied on the model were initially calculated according to conventional beam theory and then modified iteratively until the desired stress distribution was achieved. Table 1 presents the maximum displacements and rotations applied on the numerical models at the neutral axis of the beam. The stress distribution from $2\sigma_o$ to 0 through the beam section was defined by the contribution of membrane and bending stress caused by displacement and bending stress caused by rotation. The imposed

Table 1. Displacements and rotations applied on the models.

a/W	0.20	0.50
Δ (displacement)	0.1243 mm	0.2557 mm
Θ (rotation)	0.00564 rad	0.01511 rad

Table 2. Sequence of loading.

Load case	Condition	Maximum stress
1	Pressure test	$2\sigma_o$
2	Operational load	$2\sigma_o/1.3$
3	Operational load	$2\sigma_o/1.3$
4	Pressure test	$2\sigma_o$
5	Operational load	$2\sigma_o/1.3$
6	Operational load	$2\sigma_o/1.3$

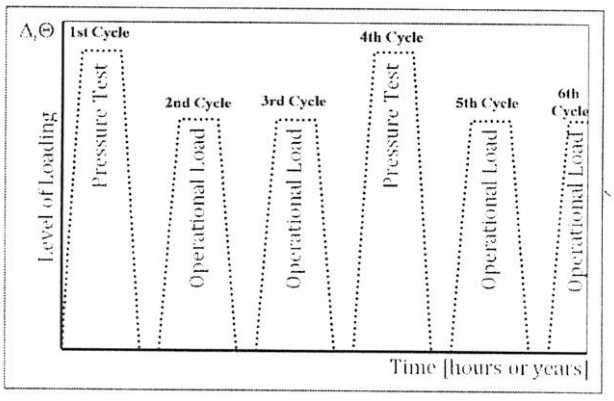

Figure 3. Sequence of loading.

stress distribution obeys the limits of ASME Code regarding primary stress below the yield strength and primary plus secondary stress below twice the yield strength.

The sequence of loading, shown in Table 2 and schematically represented in Figure 3, was applied in order to reproduce an actual condition associated with a typical load history imposed on a pressure vessel: (1) the first cycle represents a pressure test after vessel construction; (2) the second and third cycles are associated with operational condition along some years of use; (3) the fourth cycle corresponds to an extra pressure test applied due to industry regulations and (4) the fifth and sixth cycles define future operational conditions. The loading step corresponds to the pressurization phase of the equipment when axial displacement and rotation are applied according to Figure 2, and the unloading step corresponds to the depressurization phase in which the same absolute values of displacements and rotations are applied in the opposite direction. Each load cycle (pressurization or depressurization) was applied in 20 load steps, resulting in a total of 220 load steps for 5½ cycles. It should be observed that displacements and rotations are applied from zero to maximum and back to zero during unloading.

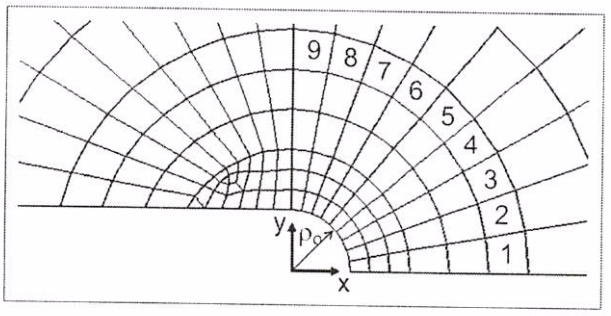

Figure 4. Crack-tip blunting.

All numerical models used in this study were automatically created with a scripting language available in the software ANSYS V14.0[27] named ANSYS Parametric Design Language (APDL) that can be used to automate common tasks or even build a specific model in terms of given parameters (variables). The APDL interface allows creating parametric files for preprocessing, finding the numerical solution and post-processing the numerical models. The *J*-integral and CTOD fracture parameters for all load steps were stored in vectors during the post-processing of the results. Additionally, the stress and strain (first, second and third principal directions, crack opening direction and equivalent Von Mises) related to a distance $r = 2J/\sigma_o$ were extracted from the generated database.

The convergence of numerical models was improved using a rounded crack tip (blunting) with a radius of 0.0025 mm and nine elements arranged along 90° as displayed in Figure 4. An important parameter related to the convergence of plastic strain vector is defined by ANSYS software as the maximum equivalent plastic strain allowed in each load step. The default for an elastic plastic analysis is 15%, which in this study was reduced to 7.5%. If the calculated value in the load step is greater than this established limit, the software performs a bisection of loading, reducing the variation to be applied on the next load step.

Constitutive models

A reliable prediction of material behavior remains essential in structural design, especially when cyclic plasticity is expected to occur. Additional difficulties may be anticipated when the material behavior cannot be adequately assessed due to lack of experiments capable of capturing the effects of cyclic strains ahead of a crack-like flaw. Therefore, the simulation of shakedown behavior may depend upon the adopted hardening model used in the numerical analysis. Regardless of uncertainties in the actual material behavior, a key ingredient in the material modeling is the incorporation of the deformation history associated with the changes in the stress and strain fields as well as with the variation of the crack driving forces and fracture parameters over the loading cycles.

Table 3. Constants of Chaboche model.

Constant	Value
C_1	2067.48
C_2	13,677.79
C_3	129,872.40
γ_1	7.32
γ_2	102.06
γ_3	1395.25

The most common theories for plastic analysis of metallic materials include the isotropic and kinematic hardening models. For all plastic flow processes where cyclic plasticity is involved, a kinematic formulation must be used to account for the Bauschinger effect that is exhibited by all ductile metallic materials under load-controlled or deformation-controlled conditions.

Bari and Hassan[28] have evaluated the ability of constitutive models to predict ratcheting, and they concluded that the linear kinematic hardening model proposed by Prager[29] as well as the nonlinear kinematic hardening model of Armstrong and Frederick[30] overpredict the strains during the initial cycles. In the same work, Bari and Hassan[28] concluded that the material model defined by Lemaitre and Chaboche[31] and Chaboche,[32,33] which primarily builds upon the superposition of several hardening rules provided by Armstrong and Frederick,[30] represents a significant improvement to describe the material's response while tracing the experimentally measured hysteresis loop very closely. A number of works[34–39] have proposed a similar approach and agree that the Chaboche model is highly effective in reproducing either a shakedown or ratcheting mechanism; however, the quality of the results is strongly associated with the calibration of the model parameters.

The material model used for the development of the numerical solutions presented here incorporates elastic plastic and kinematic hardening behavior defined by the Lemaitre and Chaboche[31] and Chaboche[32,33] model. For this specific material behavior, three material models are superposed in the form

$$\alpha = \frac{C_1}{\gamma_1}[1 - exp(-\gamma_1 \varepsilon_i^p)] + \frac{C_2}{\gamma_2}[1 - exp(-\gamma_2 \varepsilon_i^p)] + \frac{C_3}{\gamma_3}[1 - exp(-\gamma_3 \varepsilon_i^p)] \quad (10)$$

where α is the backstress, ε_i^p denotes the equivalent plastic strain and C_1, C_2, C_3, γ_1, γ_2 and γ are constants in the Chaboche model, which are presented in Table 3. These constants represent a carbon (ferritic) steel plate commonly used in construction of pressure vessels (ASTM specification A516, Grade 70). The calibration of these constants was performed using a specific routine available in ANSYS,[27] which handles the

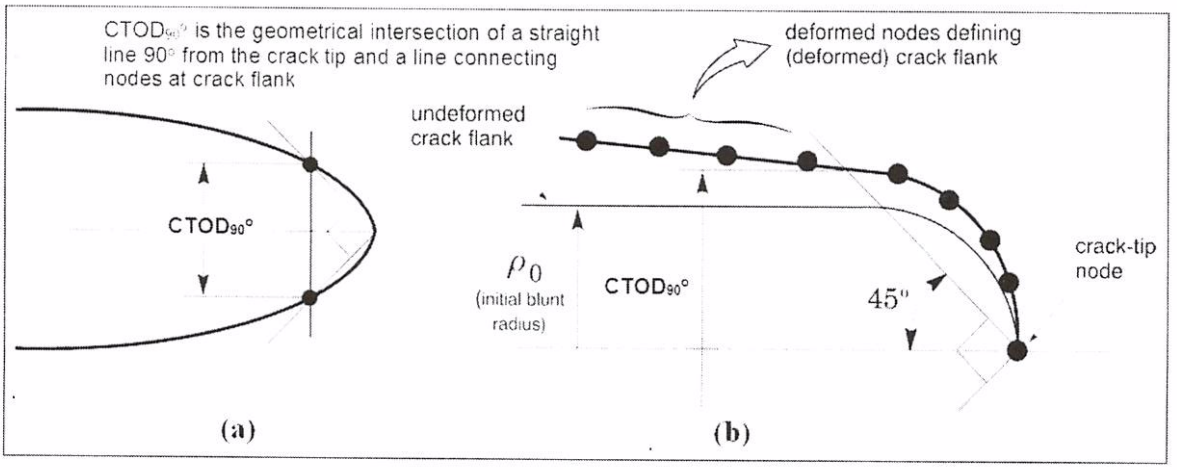

Figure 5. Procedure for CTOD determination.

Chaboche model by conducting a material curve fitting based on a nonlinear regression process. Readers are referred to ANSYS user guide[27] for additional details.

The numerical analyses for the MBL model representing the reference stress condition and the beam models representing the solution of primary and secondary stresses that develop at geometric discontinuities of pressure vessels incorporate the material behavior described above. The yield criterion follows Von Mises[40,41] for ductile metals. The mechanical properties for the adopted material are $E = 207$ GPa, $E/\sigma_o = 790$ and $n = 5.68$.

Computation of J-integral and CTOD

The value of integral J, which represents a mechanical energy release rate of crack tip, is given by[42]

$$J = \lim_{\Gamma \to 0} \int_{\Gamma} \left[W n_i - \sigma_{ij} \frac{\partial u_j}{\partial x_i} n_j \right] d\Gamma \qquad (11)$$

where Γ defines a contour beginning at the lower crack surface and ending on the upper crack surface, n_j is the outward normal to Γ, W denotes the strain energy density, σ_{ij} is the stress tensor and u_j are displacements in the coordinate system with origin at the crack tip. Numerical evaluation of equation (11) for each level of loading was accomplished by using an APDL file for post-processing the results. Previous numerical experiments revealed that this approach permits a better control and verification on intermediate results without loss of precision in the final results.

The numerical determination of CTOD follows the 90° procedure[19] to the deformed crack flanks. The approach defines the half of CTOD as the geometrical intersection of a straight line 45° from the crack tip and a line connecting the selected nodes at crack flank as shown in Figure 5. This approach simplifies the CTOD determination and provides adequate values, even if the elements at the crack tip become highly distorted.

Results and discussion

Choice of reference field

The mechanistic rationale for adopting plane-strain, high-constraint crack-tip stress fields as the *reference* stress solution lies on the rigorous correlation between the (remote) loading transmitted to the crack tip and such fields in finite bodies when the plastic zones remain vanishingly small compared to the relevant physical dimension, for example, crack length, thickness or remaining ligament.[43] Here, the plane-strain crack-tip fields associated with such restricted conditions are uniquely characterized by the J-integral. The plane-strain crack-tip fields emerging from the MBL solution using large geometry change (LGC) assumptions describe accurately the continuum stress and deformation fields averaged over micro-structurally significant length scales while enabling consideration of arbitrary material flow properties without difficulties.

Figure 6(a) compares the opening mode stresses normalized by σ_o with normalized radius, $\lambda = r/(J/\sigma_o)$, on the crack plane of the reference field obtained using (1) the HRR field, (2) a small geometry change (SGC) boundary layer analysis and (3) a LGC boundary layer analysis. The boundary layer analyses employ a description of the material's uniaxial stress strain response represented by previous equation (2) with $E/\sigma_o = 790$ and $n = 5.68$ and adopting $E = 207$ GPa and $\nu = 0.3$. Outside the blunting zone, the LGC and SGC stresses converge to very similar values (note that LGC values represent true stresses in Figure 6). This work adopts the SGC solution with the reference stress field obtained from MBL model as displayed in Figure 6(a), where $\sigma_r/\sigma_o \approx 3.85$ at the normalized distance ahead of crack tip given by $r = 2J/\sigma$.

Figure 6(b) provides the steady-state reference crack-tip fields constructed for SSY conditions with $E/\sigma_o = 790$, $n = 5.68$, $E = 207$ GPa and $\nu = 0.3$. In this figure, the distances are normalized with the factor $(K_I/\sigma_o)^2$, and the crack opening stresses are normalized

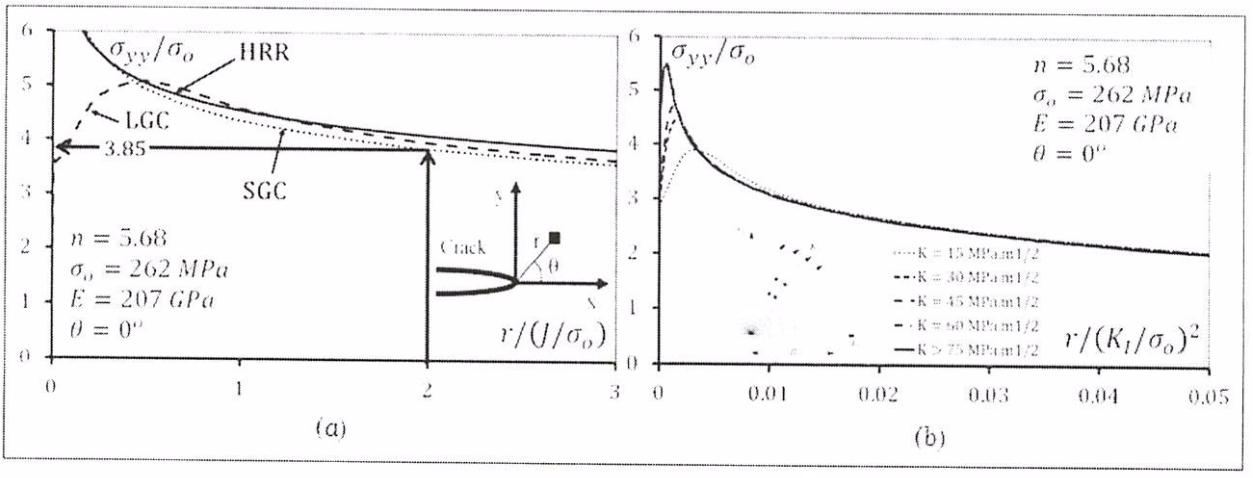

Figure 6. (a) Comparison of the HRR solution with crack-tip opening stresses for the SGC and LGC boundary analyses for n = 5.68 and E/σ_o = 790 and (b) steady-state solution of near-tip opening stresses under SSY conditions for n= 5.68 and E/σ_o = 790. HRR: Hutchinson, Rice and Rosengren; SGC: small geometry change; LGC: large geometry change.

by σ_o. At the beginning of remote applied loading, the crack-tip blunting occurs, and higher levels of near-tip stresses are developed. After a substantial increase in crack root radius which follows higher applied loads, a steady-state solution is developed, and the near-tip fields under SSY conditions are a continuous series of self-similar solutions.

J-Q trajectories incorporating shakedown effects

The extensive finite element analyses of the beam model described previously provide the basis to assess shakedown effects on crack-tip constraint for this configuration in terms of Q solutions. Figures 7 and 8 show the J-Q trajectories for the evaluated crack configuration for different a/W ratios. In these figures, the pressurizations (loadings) are represented by solid lines, while the depressurizations (unloading) are represented by dotted lines. In all plots, Q is defined by equation (9) at the normalized distance ahead of crack tip given by $r = 2J/\sigma_o$, whereas J is normalized by $b\sigma_o$, where b is the remaining crack ligament, $W-a$. In these figures, $J/(b\sigma_o)$ is plotted against $-Q$ to maintain positive scales. The material properties for these analyses were described previously in section "Constitutive models" corresponded to elastic–plastic behavior and kinematic hardening model defined by the parameters of Chaboche's model.

Consider the evolution of Q with normalized J for the beam model with a/W = 0.2 displayed in Figure 7. With increased loading (as characterized by the J-integral in this study) corresponding to the first loading cycle, the Q parameter is positive at very low J-values (note that the corresponding curve crosses the vertical axis of the plot at $J/(b\sigma_o) \approx 0.001$) and gradually takes on negative values with increased J-values. These results are similar to the J-Q trajectories for conventional fracture specimens given by Nevalainen and Dodds[44] and Cravero and Ruggieri.[45] After reaching

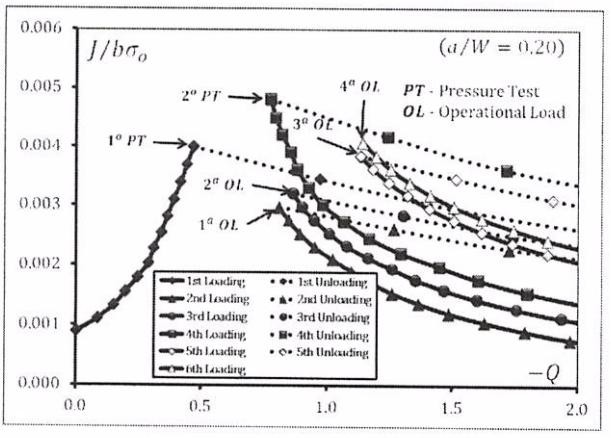

Figure 7. Evolution of parameters $-Q$ and $J/b\sigma_o$ for Model I (a/W = 0.20).

the peak load at termination of the first pressure test (marked by the arrow indicated in the plot), unloading takes place accompanied by development of reversed plasticity. Here, parameter Q falls rapidly, even with slightly decreased levels of J, in the wake of the reduced opening stresses that develop following unloading. While the next loading–unloading sequences yield qualitatively similar patterns associated with the J-Q trajectories, we note that the subsequent peak loads are described by different conditions in terms of the scalar parameters (J, Q). In particular, the peak load for the second pressure test is described by the scalar parameters (J, Q), which differ significantly from the corresponding J-Q values defining the peak load for the first pressure test. Now, direct attention to the variation of Q with normalized J for the beam model with a/W = 0.5 is displayed in Figure 8. The key features associated with the evolution of parameter Q with the loading–unloading cycles remain essentially unchanged. However, note that because of the dependence of J on crack size, the levels of $J/(b\sigma_o)$ attained in the beam

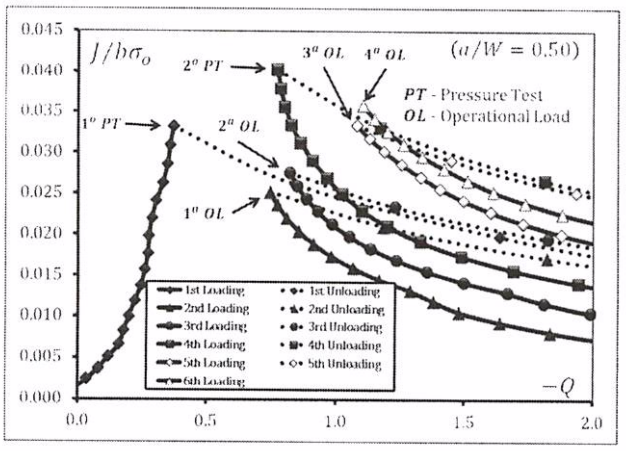

Figure 8. Evolution of parameters $-Q$ and $J/b\sigma_o$ for Model 2 ($a/W = 0.50$).

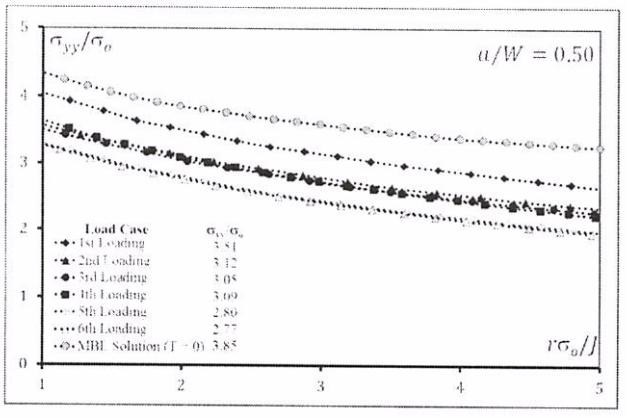

Figure 9. Stress distribution for crack opening at the end of pressurization steps.
MBL: modified boundary layer.

model with $a/W = 0.5$ are higher than the analyses with $a/W = 0.2$.

Figure 9 shows the crack opening stress distribution at the end of each pressurization for the high-constraint level condition ($a/W = 0.5$). It may be observed that the curves are approximately parallel to MBL solution. Such feature confirms one important assumption of a two-parameter fracture mechanics approach based on the J-Q methodology: an uniform hydrostatic stress distribution in the interval $J/\sigma_o \leqslant r \leqslant 5J/\sigma_o$.

The effect of shakedown on the fracture behavior of a crack subjected to pressure load cycles is amply demonstrated by the evolution of J-Q trajectories with load cycles displayed in Figures 7 and 8. The preceding results indicate that the plasticity development associated with loading, unloading and reloading actually increases the material's resistance against brittle fracture. This can be understood in terms of the role played by parameter Q in relation to the amplitude of the near-tip stresses. As discussed previously by O'Dowd and Shih,[20,21] in a highly constrained condition corresponding to nonnegative Q-values, the tensile (opening) crack-tip stresses are high and follow closely the stress distribution described by the MBL solution provided in

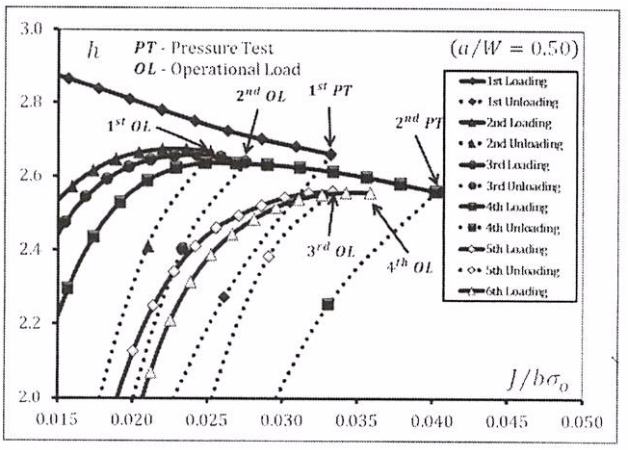

Figure 10. Evolution of parameter J and level of triaxiality factor h ($a/W = 0.50$).

section "High-constraint reference field based on the MBL model," as well the HRR stress field. However, as the crack-tip constraint is relaxed with increased negative Q-values, the tensile near-tip stresses fall gradually below the high-constrained MBL values, thereby making it more difficult for the crack to propagate unstably. Note that this is exactly the conclusion that can be drawn from the analysis of the peak load attained at termination of the second pressure test in both plots.

Figure 10 shows the triaxiality parameter defined by $h = \sigma_{avg}/\sigma_{vm}$, where σ_{avg} is the hydrostatic stress and σ_{vm} is the equivalent stress (Von Mises). It is seen that the triaxiality parameter, h, remains approximately constant after applying cycles of loading, which contrasts sharply to the J-Q behavior previously discussed. Therefore, it can be concluded that the triaxiality parameter, h, has limited utility to characterize constraint variations in the present analyses, mainly due the limited number of cycles applied on the model.

Another important feature arising from this work is associated with the contribution term to the increase in the crack driving force as characterized by the J-integral. A numerical evaluation of results shown in Figure 8 indicates an increase of 20.4% in the crack driving force ($J/b\sigma_o$) when the first pressure test and second pressure test are compared. Indeed, for all load cases, similar results may be observed, especially after application of second pressure test which induces a higher percentual variation of $J/b\sigma_o$ (32.4%), if the third operational load and the second operational load are compared. Here, it is not fully evident whether the crack is critical or not critical for initiating subcritical tearing after application of a number of pressurization cycles and strain accumulation. To explain how the J-integral increases in a cycle-by-cycle manner, the individual contributions of the previous equation (11) were determined as follows: the first term, named here as J_A, defined by

$$J_A = \lim_{\Gamma \to 0} \int_{\Gamma} [Wn_1] d\Gamma \qquad (12)$$

Table 4. Values of J_A and J_B along cycles of loading ($a/W = 0.50$).

Load condition	Identification	J_A (kJ/m^2)	J_B (kJ/m^2)	$J = J_A - J_B$ (kJ/m^2)
First pressure test	First pressurization	18.7	−199.9	218.6
Second operational load	Second pressurization	26.0	−129.2	155.2
Second operational load	Third pressurization	34.1	−130.0	164.1
Second pressure test	Fourth pressurization	46.9	−195.1	242.0
Third operational load	Fifth pressurization	55.1	−130.5	185.6
Fourth operational load	Sixth pressurization	63.3	−131.5	194.8

is related to plastic level, while the second term, named as J_B, defined by

$$J_B = \lim_{\Gamma \to 0} \int_{\Gamma} \left[\sigma_{ij} \frac{\partial u_i}{\partial x_i} n_j \right] d\Gamma \tag{13}$$

is related to elastic energy variation. Table 4 shows the computed results where it may be observed that the first term increases due to plastic strain accumulation near the crack tip, while the second term remains proportional to the loading level.

Evolution of crack-tip constraint with load history based on CTOD

Much previous research work has demonstrated[43] that until large-scale plasticity develops in cracked structural components, the evolving crack-tip stress field has essentially the structure of the plane-strain, SSY stress fields.[44] While such SSY conditions prevail, the J-integral provides a single-parameter characterization of the near-tip stress and strain fields. Furthermore, by relating J and the CTOD[19,46] as

$$\mathrm{CTOD} = \frac{d_n J}{\sigma_o} \tag{14}$$

it becomes clear that a similar conclusion also holds true when the CTOD is adopted to characterize the crack-tip driving force. However, under cyclic load and reversed plasticity, such as during a shakedown process addressed in the previous section, the above relationship between J and CTOD given by equation (14) may not necessarily hold true. Because the CTOD is a geometric crack-tip parameter rather than a measure of crack-tip strain energy upon loading such as the J-integral, the variation of crack driving force in terms of parameter CTOD with the loading–unloading sequences may reflect load history effects in a different manner.

Figure 11 displays the relationship between parameters of fracture J and CTOD along 5½ cycles of loading. While the parameter J goes to zero during depressurization, the CTOD remains consistently above a minimum value, which is most likely related to residual stress developed during shakedown process. It is interesting to observe that curve slope for the first loading is approximately the same for other loadings indicating that, in spite of changes in constraint and cycles of unloading, the CTOD-value defined by equation (14) is not significantly altered at the end of the loading steps.

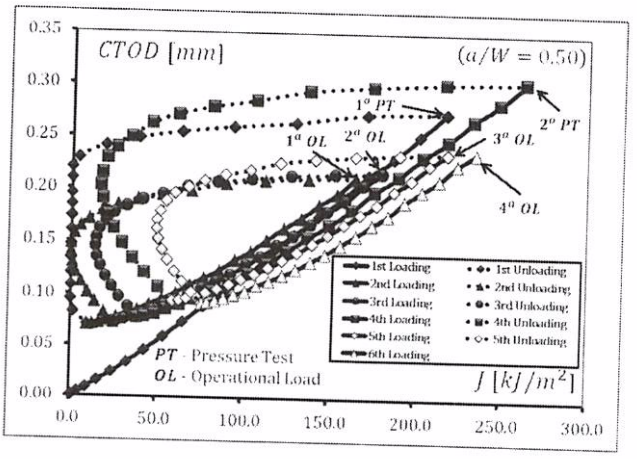

Figure 11. Evolution of parameters J and CTOD for Model 2 ($a/W = 0.50$).
CTOD: crack-tip opening displacement.

Concluding remarks

It is possible to conclude based on the results presented in this work that a two-parameter fracture mechanics approach based on J-Q provides a consistent framework for evaluating cracks located in geometrical discontinuities of pressure vessels submitted to few pressurization and depressurization cycles representing actual operational conditions (pressure tests and operational loadings). Relevant changes in crack driving forces and levels of constraint for crack-like flaws submitted to alternating membrane and bending stress were also observed, even for global stress range inside shakedown limits. Such behavior is related to higher levels of plastic strains close to the crack tip and increased accumulated deformation energy. The analyses enable capturing this effect by describing the material behavior in terms of a kinematic hardening model defined by Chaboche parameters. Finally, it may be observed that a lower probability of unstable fracture may be assumed for ductile and high-toughness materials after applied few cycles of pressurization and depressurization. However, due to the increase in the crack driving force, it is not completely evident whether the crack is critical for initiating a subcritical tearing.

Assuming that the material toughness is high enough to avoid any crack ductile tearing during pressurization and depressurization cycles, the observed phenomena close to the crack tip may be compared to strain instability when shakedown is not guaranteed.

Acknowledgement

One of the authors (J.M.A.R.) expresses his acknowledgements to the Brazilian Council for Scientific and Technological Development (CNPq).

Declaration of conflicting interests

The authors declare that there is no conflict of interest.

Funding

This investigation is supported by PETROBRAS—Brazilian Oil Company, as part of a Thesis of Doctor of Sciences submitted to the Department of Metallurgy and Materials Engineering of Federal University of Rio de Janeiro, Brazil, in cooperation with the Department of Naval Architecture and Ocean Engineering of São Paulo University, Brazil.

References

1. Westergaard HM. Bearing pressures and cracks. *J Appl Mech: T ASME* 1939; 6: 49–53.
2. Williams ML. On the stress distribution at the base of a stationary crack. *J Appl Mech* 1957; 24: 109–114.
3. Wells AA. Unstable crack propagation in metals: cleavage and fast fracture. In: *Proceedings of the crack propagation symposium*. College of Aeronautics, Cranfield, UK. September 1961. vol. 1. paper 84.
4. Rice JR. A path independent integral and the approximate analysis of strain concentration by notches and cracks. *J Appl Mech: T ASME* 1968; 35: 379–386.
5. Melan E. Zur plastizitat des raumluchen kontinuums. *Ing Arch* 1938; 9: 116–126.
6. Yu MA. *Generalized plasticity*. New York: Springer-Verlag, 2006.
7. Abdel-Karim M. Shakedown of complex structures according to various hardening rules. *Int J Pres Ves Pip* 2005; 82: 427–458.
8. Konig JA. *Shakedown of elastic-plastic structural*. New York: Elsevier Science Publishing, 1987.
9. Konig JA and Maier G. Shakedown analysis of elastic-plastic structures: a review of recent developments. *Nucl Eng Des* 1981; 66: 81–95.
10. Sawczuk A. Shakedown analysis of elastic-plastic structures. *Nucl Eng Des* 1974; 28: 121–136.
11. The American Society of Mechanical Engineers. *ASME boiler and pressure vessel code* (Section VIII, Division 2). New York: ASME, 2010.
12. Stein E, Zhang G, Huang Y, et al. Theoretical and computational shakedown analysis of non-linear kinematic hardening material and transition to ductile fracture. In: Steck E, Ritter R, Peil U, et al. (eds) *Plasticity of metals: experiments, models, computation: Collaborative Research Centres*. Federal Republic of Germany: Wiley-VCH, 2001, pp.253–274.
13. Feng X-Q and Gross D. A global/local shakedown analysis method of elastoplastic cracked structures. *Eng Fract Mech* 1997; 63: 179–192.
14. Hutchinson JW. Singular behavior at the end of a tensile crack in a hardening material. *J Mech Phys Solids* 1968; 16: 13–31.
15. Hutchinson JW. Plastic stress and strain fields at a crack tip. *J Mech Phys Solids* 1968; 16: 337–347.
16. Rice JR and Rosegren GF. Plane strain deformation near a crack tip in a power-law hardening material. *J Mech Phys Solids* 1968; 16: 1–12.
17. Rice JR. *Mathematical analysis in the mechanics of fracture*. New York: Academic Press, 1968.
18. Anderson TL. *Fracture mechanics: fundaments and applications*. 3rd ed.Boca Raton, FL: CRC Press, 2005.
19. Rice JR. Mechanics of crack tip deformation and extension by fatigue. In: Grosskreutz J (ed.) *Fatigue crack propagation* (ASTM STP 415). West Conshohocken, PA: American Society for Testing and Materials, 1967, pp.247–311.
20. O'Dowd N and Shih C. Family of crack-tip fields characterized by a triaxiality parameter: part I. Structure of fields. *J Mech Phys Solids* 1991; 39: 989–1015.
21. O'Dowd N and Shih C. Family of crack-tip fields characterized by a triaxiality parameter: part II. Fracture applications. *J Mech Phys Solids* 1992; 40: 939–963.
22. Larsson SG and Carlsson AJ. Influence of non-singular stress terms and specimen geometry on small scale yielding at crack-tip in elastic-plastic materials. *J Mech Phys Solids* 1973; 21: 447–473.
23. Rice JR. Limitations to the small scale yielding approximation for crack tip plasticity. *J Mech Phys Solids* 1974; 22: 17–26.
24. Dodds RH, Shih C and Anderson TL. Continuum and micromechanics treatment of constraint in fracture. *Int J Fracture* 1993; 64: 101–133.
25. BS 7910:2005. Guide on methods for assessing the acceptability of flaws in metallic structures (BSI—British Standards).
26. API 579/ASME FFS-1:2007. Fitness-for-service (American Petroleum Institute).
27. ANSYS, Inc. *ANSYS structural mechanics software V14.0*. Canonsburg, PA: ANSYS, Inc., 2013.
28. Bari S and Hassan T. Anatomy of coupled constitutive models for ratcheting simulation. *Int J Plasticity* 2000; 16: 381–409.
29. Prager W. A new method of analyzing stress and strain in work hardening plastic solids. *J Appl Mech: ASME* 1956; 78: 493.
30. Armstrong PJ and Frederick CO. *A mathematical representation of the multiaxial Bauschinger effect*. CEGB Report, RD/B/N731, 1966. UK: Berkeley Nuclear Laboratories.
31. Lemaitre J and Chaboche JL. *Mechanics of solid materials*. Cambridge: Cambridge University Press, 1990.
32. Chaboche JL. Constitutive equations for cyclic plasticity and cyclic viscoplasticity. *Int J Plasticity* 1989; 5: 247–302.
33. Chaboche JL. On some modifications of kinematic hardening to improve the description of ratcheting effects. *Int J Plasticity* 1991; 7: 661–678.
34. Rezaiee-Pajand M and Sinaie S. On the calibration of the Chaboche hardening model and a modified hardening

rule for uniaxial ratcheting prediction. *Int J Solids Struct* 2009; 46: 3009–3017.
35. Kulkarni SC, Desai YM, Kant T, et al. Uniaxial and biaxial ratcheting in piping materials. *Int J Pres Ves Pip* 2004; 81: 609–617.
36. Chellapandi P, Ramesh R, Chetal SC, et al. Application of Chaboche viscoplastic theory for predicting the cyclic behaviour of modified 9Cr-1Mo. In: *Transactions of the 14th international conference on structural mechanics in reactor technology (SMiRT 14)*. Lyon, 17–22 August 1997, pp.67–76.
37. Broggiato GB, Campana F and Cortese L. The Chaboche nonlinear kinematic hardening model: calibration methodology and validation. *Meccanica* 2008; 43: 115–124.
38. Shojaei A, Eslami MR and Mahbadi H. Cyclic loading of beams based on the Chaboche model. *Int J Mech Mater Des* 2010; 6: 217–228.
39. Mahmoudi AH, Badnava H and Pezeshki-Najafabadi M. An application of Chaboche model to predict uniaxial and multiaxial ratcheting. *Proced Eng* 2011; 10: 1924–1929.
40. Chakrabarty J. *Theory of plasticity*. 3rd ed.Oxford: Elsevier Butterworth-Heinemann, 2006.
41. Chen WF and Han DJ. *Plasticity for structural engineers*. Fort Lauderdale, FL: J. Ross Publishing, 2007.
42. Moran B and Shih CF. A general treatment of crack tip contour integrals. *Int J Fracture* 1987; 35: 295–310.
43. Hutchinson JW. Fundamentals of the phenomenological theory of nonlinear fracture mechanics. *J Appl Mech: T ASME* 1983; 50: 1042–1051.
44. Nevalainen M and Dodds RH. Numerical investigation of 3-D constraint effects on brittle fracture in SE(B) and C(T) specimens. *Int J Fracture* 1995; 74: 131–161.
45. Cravero S and Ruggieri C. Correlation of fracture behavior in high pressure pipeline with axial flaws using constraint designed test specimens: part I. Plane strain analyses. *Eng Fract Mech* 2005; 72: 1344–1360.
46. Shih CF. Relationship between the *J*-integral and the crack opening displacement for stationary and extending cracks. *J Mech Phys Solids* 1981; 29: 305–326.

The Journal of Strain Analysis for Engineering Design
http://sdj.sagepub.com/

A two-parameter approach to assess effects of constraint in cracks located at geometrical discontinuities

Guilherme Victor P Donato, João Marcos A Rebello and Claudio Ruggieri

The Journal of Strain Analysis for Engineering Design published online 13 March 2014
DOI: 10.1177/0309324714525146

The online version of this article can be found at:
http://sdj.sagepub.com/content/early/2014/03/11/0309324714525146

Published by:
SAGE
http://www.sagepublications.com

On behalf of:
Institution of Mechanical Engineers